ASTRONOMY & ASTROPHYSICS
SUPPLEMENT SERIES

JANUARY II **2000**, PAGE 285

Astron. Astrophys. Suppl. Ser. **141**, 285–296 (2000)

Atomic data from the IRON Project

XL. Electron impact excitation of the Fe XIV EUV transitions

P.J. Storey[1], **H.E. Mason**[2], **and P.R. Young**[2]

[1] Department of Physics and Astronomy, Gower Street, London WC1E 6BT, UK
[2] Department of Applied Mathematics and Theoretical Physics, Silver Street, Cambridge CB3 9EW, UK

Received April 26; accepted August 26, 1999

Abstract. We calculate collision strengths and thermally averaged collision strengths for electron excitation between the forty energetically lowest levels of Fe^{13+}. The scattering calculation is more complete than any previous work on this ion and significant differences are found in the excitation rates for many of the extreme ultra-violet (EUV) transitions, compared to earlier work. A detailed comparison is made between predicted line intensity ratios and those observed in solar coronal spectra which shows that several outstanding discrepancies are resolved by the new atomic data.

Key words: Sun: corona; atomic data; UV radiation

1. Introduction

Fe XIV is one of the most important diagnostic ions in the solar corona. It is abundant at a temperature of about 2 10^6 K (Arnaud & Raymond 1992). Transitions within Fe XIV give rise to spectral lines in the visible (green line, 5303 Å) and extreme ultraviolet (EUV) wavelength ranges. The visible line which arises from the forbidden transition ($3s^23p$, $^2P^o_{1/2}-^2P^o_{3/2}$) was discussed in Storey et al. (1996) (hereafter IP XIV). In this paper we consider the transitions between the ground configuration ($3s^23p$) and excited configurations ($3s3p^2$, $3s^23d$ and $3s3p3d$). The EUV lines can be used to determine electron density in the solar atmosphere, as with recent observations from the Solar and Heliospheric Observatory (SOHO) (Mason et al. 1997).

In IP XIV, a review was given of the early calculations carried out for Fe XIV, while Mason (1994) (hereafter M 94) has critically compared the existing calculations. She found that the results presented by Dufton & Kingston (1991) (hereafter DK91) were limited in two respects – they only used a 3 configuration target and the averaged collision strengths were obtained using LS-coupling collision strengths below 10 Ryd. She recommended using the DK91 atomic data with caution, but suggested that new calculations should be carried out with a more extensive target and in intermediate coupling. Bhatia & Kastner (1993) (hereafter BK93) provide distorted wave calculations for Fe XIV with an extensive target. An analysis of the solar EUV lines using these new data was published by Bhatia et al. (1994) (hereafter B94) and contained new identifications for several spectral lines. There remain some longstanding inconsistencies between the theoretical and observed intensity ratios as detailed by Young et al. (1998) (hereafter Y98) indicating that more accurate close coupling (CC) calculations are required.

This work is part of the international collaboration known as the Iron Project (Hummer et al. 1993) whose aim is to make systematic calculations of electron scattering cross-sections and rate coefficients for ions of astronomical interest, using the best available methods. The principal tool of the project is the atomic R-matrix computer code of Berrington et al. (1974, 1978) as extended for use in the Opacity Project (Berrington et al. 1987). These codes have recently been further extended (Hummer et al. 1993) so that collision strengths can be calculated at low energies, where some scattering channels are closed, including the effects of intermediate coupling in the target. Previous calculations have always neglected such effects.

In Sect. 2, we discuss the target used in our Fe XIV model. We give details of the electron scattering calculations in Sect. 3 and make a critical comparison with previous work in Sect. 4. The calculated line intensities and level populations are given in Sect. 5 and Sect. 6. Our theoretical intensity ratios are compared with those from solar observations in Sect. 7.

Send offprint requests to: P.J. Storey

Table 1. Energies of target terms in Rydberg

Term		Exp.†	Basis 1	Basis 2
$3s^23p$	$^2P^o$	0.	0.	0.
$3s3p^2$	^4P	2.03888	2.018	2.024
	^2D	2.62454	2.619	2.625
	^2S	3.20880	3.268	3.282
	^2P	3.47445	3.488	3.502
$3s^23d$	^2D	4.20862	4.292	4.287
$3p^3$	$^2D^o$	5.15891	5.154	5.173
	$^4S^o$	5.25285	5.259	5.281
	$^2P^o$	5.75764	5.744	5.763
3s3p3d	$^4F^o$	5.82870*	5.845	5.860
	$^4P^o$	6.23865	6.273	6.289
	$^4D^o$	6.26927	6.302	6.315
	$^2D^o$	6.42468	6.458	6.473
	$^2F^o$	6.75142	6.829	6.844
	$^2P^o$	7.26477	7.375	7.391
	$^2F^o$	7.34768	7.475	7.469
	$^2P^o$	7.56079	7.681	7.696
	$^2D^o$	7.56742	7.681	7.697

† Churilov & Levashov (1993), Redfors & Litzén (1989).
* Not all levels known experimentally.

Table 2. Weighted oscillator strengths, gf

Transition			Basis 1	Basis 2	Basis 3
$3s^23p\ ^2P^o$	–	$3s3p^2\ ^2D$	0.378	0.381	0.375
	–	$3s3p^2\ ^2P$	0.320	0.325	0.319
	–	$3s3p^2\ ^2S$	2.508	2.477	2.457
	–	$3s^23d\ ^2D$	2.942	2.877	2.833

2. The target

In IP XIV we used an eighteen state target comprising all the terms of the $3s^23p$, $3s3p^2$, $3s^23d$, $3p^3$ and 3s3p3d electron configurations. These states were expanded in a seventeen configuration basis which included some configurations containing $n = 4$ orbitals. Full details of the composition of that target and the computer codes used to generate it are given in IP XIV. In this paper, we will use the same target as described in IP XIV when dealing with the resonance region, where some scattering channels are closed. In the region of all channels open, above our highest target threshold, we use a simpler target, which contains no $n = 4$ orbitals. This was necessary due to the appearance of physically dubious resonances in the open channel region, caused by electron configurations in the target expansion containing $n = 4$ orbitals, but with no associated target states.

The simpler target basis consists of the nine electron configurations of the $n = 3$ complex and, as in IP XIV, the target radial wavefunctions were calculated with the general purpose atomic structure code SUPERSTRUCTURE (Eissner et al. 1974; Nussbaumer & Storey 1978). The scaling parameters for the statistical model potentials for the six orbitals 1s to 3d inclusive are 1.40465, 1.10939, 1.05182, 1.11193, 1.08085, 1.08479. As in IP XIV, the calculation of the target wavefunctions is carried out in LS-coupling, but with the one-body mass and Darwin relativistic energy shifts included. Incorporating these shifts leads to better agreement between the calculated and the experimental energies, without the greatly increased computational cost of carrying out the scattering calculation including fine-structure interactions. In Table 1, we compare the calculated term energies from this calculation (Basis 1) with experiment and with the larger target described in IP XIV (Basis 2). In Table 2, we

Table 3. Energies of target levels in Rydberg

Index	Config.	Level	Calculated	Experimental†
1	$3s^2$ 3p	$^2P^o_{1/2}$	0.00000	0.00000
2		$^2P^o_{3/2}$	0.16850	0.17179
3	3s $3p^2$	$^4P_{1/2}$	2.02729	2.05139
4		$^4P_{3/2}$	2.09568	2.12133
5		$^4P_{5/2}$	2.18229	2.20880
6		$^2D_{3/2}$	2.73082	2.72689
7		$^2D_{5/2}$	2.74989	2.74719
8		$^2S_{1/2}$	3.36257	3.32333
9		$^2P_{1/2}$	3.58371	3.54036
10		$^2P_{3/2}$	3.65713	3.61328
11	$3s^2$ 3d	$^2D_{3/2}$	4.38676	4.31233
12		$^2D_{5/2}$	4.40889	4.33036
13	$3p^3$	$^2D^o_{3/2}$	5.25464	5.25239
14		$^2D^o_{5/2}$	5.28780	5.28747
15		$^4S^o_{3/2}$	5.37640	5.36738
16	3s 3p 3d	$^4F^o_{3/2}$	5.87685	
17	$3p^3$	$^2P^o_{1/2}$	5.88362	5.85197
18		$^2P^o_{3/2}$	5.91009	[a]5.88152
19	3s 3p 3d	$^4F^o_{5/2}$	5.91332	5.88668
20		$^4F^o_{7/2}$	5.96590	5.94097
21		$^4F^o_{9/2}$	6.03878	6.01676
22		$^4P^o_{5/2}$	6.33538	6.29051
23		$^4D^o_{3/2}$	6.35618	6.31200
24		$^4D^o_{1/2}$	6.37066	6.32573
25		$^4D^o_{7/2}$	6.45619	6.40979
26		$^4P^o_{1/2}$	6.44598	6.41304
27		$^4D^o_{5/2}$	6.45759	6.41636
28		$^4P^o_{3/2}$	6.45342	6.41723
29		$^2D^o_{3/2}$	6.59249	6.53556
30		$^2D^o_{5/2}$	6.59785	6.54163
31		$^2F^o_{5/2}$	6.88292	6.78862
32		$^2F^o_{7/2}$	7.01333	6.92394
33		$^2P^o_{3/2}$	7.46965	7.35496
34		$^2P^o_{1/2}$	7.54320	7.42797
35		$^2F^o_{7/2}$	7.57352	7.45046
36		$^2F^o_{5/2}$	7.59829	7.47787
37		$^2P^o_{1/2}$	7.79103	7.65002
38		$^2D^o_{3/2}$	7.80163	7.66171
39		$^2P^o_{3/2}$	7.82900	7.68796
40		$^2D^o_{5/2}$	7.83024	7.69544

† Churilov & Levashov (1993).
[a] Redfors & Litzén (1989).

Table 4. Transition probabilities (A_{ji}, units s^{-1}) calculated with the Basis 3 target. The indices (j, i) correspond to the levels as shown in Table 3

j	i	A_{ji}	j	i	A_{ji}	j	i	A_{ji}	j	i	A_{ji}	j	i	A_{ji}
2	1	6.023(+01)	15	3	6.247(+09)	20	5	2.939(+08)	29	6	3.054(+10)	34	10	3.954(+09)
3	1	2.671(+07)	15	4	1.184(+10)	20	7	1.058(+06)	29	7	2.751(+09)	34	11	2.796(+08)
3	2	9.889(+06)	15	5	1.597(+10)	20	12	6.247(+06)	29	8	3.493(+08)	35	5	3.234(+08)
4	1	5.662(+05)	15	6	1.092(+08)	21	5	1.599(+01)	29	9	9.248(+08)	35	7	2.811(+10)
4	2	6.218(+06)	15	10	6.445(+07)	21	7	2.683(+01)	29	10	4.386(+08)	35	12	2.223(+10)
5	2	2.649(+07)	16	3	1.527(+07)	21	12	2.652(-01)	29	11	4.071(+08)	36	6	2.721(+10)
6	1	2.382(+09)	16	4	1.375(+08)	22	4	2.584(+10)	30	4	5.057(+08)	36	7	1.503(+09)
6	2	7.321(+07)	16	6	4.510(+07)	22	5	2.374(+09)	30	5	1.028(+08)	36	10	3.756(+08)
7	2	1.912(+09)	16	7	4.081(+08)	22	6	4.904(+07)	30	6	3.833(+09)	36	11	2.259(+10)
8	1	1.777(+10)	16	8	5.542(+07)	22	7	1.082(+09)	30	7	2.901(+10)	36	12	7.914(+08)
8	2	1.147(+09)	16	9	1.127(+06)	22	10	3.726(+07)	30	10	8.445(+08)	37	8	1.565(+10)
9	1	1.326(+10)	16	10	5.636(+07)	22	12	2.998(+07)	30	11	1.249(+08)	37	9	9.055(+09)
9	2	2.103(+10)	16	11	3.236(+06)	23	3	2.810(+10)	30	12	3.205(+08)	37	10	1.073(+10)
10	1	7.598(+09)	17	3	1.688(+07)	23	4	6.613(+09)	31	4	7.362(+07)	37	11	2.746(+10)
10	2	3.291(+10)	17	4	2.481(+07)	23	5	7.461(+08)	31	5	3.631(+07)	38	7	2.781(+08)
11	1	3.557(+10)	17	6	1.207(+10)	23	6	5.036(+08)	31	6	1.277(+10)	38	8	8.165(+07)
11	2	8.002(+09)	17	8	9.183(+07)	24	3	4.042(+10)	31	7	2.752(+09)	38	9	4.517(+10)
12	2	3.969(+10)	17	9	3.222(+09)	24	4	9.557(+08)	31	11	1.316(+09)	38	10	1.625(+08)
13	3	2.747(+08)	17	10	6.777(+08)	25	5	4.042(+10)	31	12	3.337(+08)	38	11	4.520(+09)
13	4	2.248(+08)	18	3	2.212(+08)	25	7	3.258(+08)	32	5	4.364(+08)	38	12	1.755(+10)
13	5	7.371(+08)	18	4	4.142(+08)	26	4	2.791(+10)	32	7	1.615(+10)	39	6	3.357(+08)
13	6	2.089(+09)	18	5	2.020(+08)	26	6	4.287(+07)	32	12	1.949(+09)	39	7	1.289(+08)
13	7	9.032(+08)	18	6	1.278(+09)	27	4	9.820(+09)	33	3	2.866(+08)	39	8	6.130(+09)
13	8	3.796(+08)	18	7	9.081(+09)	27	5	2.724(+10)	33	8	4.030(+10)	39	9	3.011(+09)
13	9	4.759(+08)	18	8	1.692(+09)	27	6	1.106(+08)	33	9	3.407(+08)	39	10	3.256(+10)
13	10	2.417(+07)	18	10	2.562(+09)	27	7	7.155(+07)	33	10	9.691(+09)	39	11	1.651(+10)
13	11	6.511(+06)	19	4	1.598(+08)	28	4	1.979(+10)	33	11	6.513(+08)	39	12	1.001(+10)
14	5	9.498(+07)	19	5	8.858(+07)	28	5	1.212(+10)	33	12	3.253(+08)	40	10	5.810(+10)
14	6	3.072(+08)	19	6	1.388(+06)	28	6	1.012(+08)	34	3	1.279(+08)	40	11	3.304(+08)
14	7	2.947(+09)	19	7	8.428(+07)	28	7	9.150(+07)	34	6	2.538(+08)	40	12	1.915(+10)
14	10	6.666(+08)	19	10	5.646(+05)	29	3	4.833(+08)	34	8	1.436(+10)			
14	12	7.708(+06)	19	11	4.990(+06)	29	4	5.457(+07)	34	9	2.690(+10)			

give gf values for the strongest allowed transitions from the ground state obtained with Basis 1 and Basis 2 and from the much larger "extended basis" described in detail in IP XIV (Basis 3), which we use as a benchmark for the accuracy of the other calculations. The largest difference in gf between Bases 1 and 3 is 3.8%, while the average difference is 1.8%. In the region of all channels open, where we use a target from Basis 1, the collision strengths for the strong allowed transitions are increasingly dominated by contributions from high partial waves whose contribution is directly proportional to the oscillator strength in the transition.

In Table 3 we give a list of the forty levels arising from the eighteen target terms, together with their calculated and experimental energies where these are known (Churilov & Levashov 1993; Redfors & Litzén 1989). The calculations were made in Basis 2 and include the one- and two-body fine-structure interactions described by Eissner et al. (1974). The levels are given in the experimental energy order. Table 3 serves as a key to the levels for use in later tabulations of collision strengths and effective collision strengths. In Sect. 6 we shall calculate the emissivities of the transitions arising from these levels. For this purpose we will use transition probabilities computed using our most extended basis, Basis 3. The results are in Table 4, where we give the Einstein A-values for the strongest transitions from each upper level. A transition is excluded if the A-value is less than 0.1 percent of the total A-value from that particular upper state. The calculation of the A-values includes empirical corrections to the Hamiltonian of the system as described by Zeippen et al. (1977), whose purpose is to bring the computed level energies into agreement with the experimental values.

3. The scattering calculation

The R-matrix method used in this calculation is described fully elsewhere (Hummer et al. 1993 and references therein). As outlined above, we include mass and Darwin relativistic energy shifts, but not the one- and two-body fine-structure interactions. For the calculation in the resonance region, we use an R-matrix boundary radius of 4.66 a.u., to encompass the most extended target orbital (4d), while in the open channel region a boundary radius of only 2.84 a.u. was required. The expansion of each scattered electron partial wave is over a basis of 22 functions within the R-matrix boundary, and the partial wave expansion extends to a maximum of $l = 15$. The outer region calculation is carried out using the program STGFJ (Hummer et al. 1993), which calculates reactance matrices in LS-coupling and then transforms them into the

Jk-coupling scheme (Saraph 1972, 1978), including the effects of intermediate coupling between the target terms, using the so-called term-coupling coefficients (TCCs).

Collision strengths in the resonance region are computed at 10000 points equally spaced in energy. We do not, therefore attempt to delineate all resonance structures fully. The accuracy of this sampling approach was discussed in IP XIV, where it was concluded that this number of points should lead to a purely statistical error of less than 1%. In the region of all channels open, a further 125 points span the energy range from the highest threshold up to 100 Ryd.

For energies above the highest threshold, the partial wave expansion extends to $l = 18$ and the collision strengths are corrected for missing partial waves using the method described by Binello et al. (1998). In brief, for optically allowed transitions contributions from partial waves $l > 18$ are calculated in the Coulomb-Bethe approximation, using oscillator strengths taken from the Basis 1 target calculation including fine-structure effects. For the remaining transitions, the contribution from the high partial waves is estimated by assuming that the partial collision strengths are declining geometrically as a function of partial wave. Once all collision strengths have been corrected for missing partial waves, they are extrapolated to energies higher than 100 Ryd using the high energy behaviours discussed by Burgess & Tully (1992). Further details are given in Binello et al. (1998).

4. Results and discussion

In Table 5 we compare our total collision strengths between the the two levels of the ground term and the levels of the two even parity configurations $3s3p^2$ and $3s^23d$, with the work of BK93 and the values given by M 94. At the energies given in Table 5, (10 and 30 Ryd) none of the calculations contain any resonance features. The results of BK93 were obtained using the distorted wave method supplemented by the Coulomb-Bethe method for high partial waves. Their target basis contained only the five electron configurations given in Table 1 and their calculations were made at 10, 20 and 30 Ryd, above all thresholds. The agreement is generally good, as one would expect at these relatively high energies, with an average difference at 10 Ryd of 16.9%. The values quoted in M 94 at 10 Ryd are data computed by Dufton and Kingston in 1982 and deposited in the Belfast atomic databank. The calculations were made in the close-coupling approximation (see DK91 for more details). Again the agreement with the present work is good, with an average difference of 13.5%. Most of the difference between the present work and the other two calculations is attributable to the large differences for the strong allowed transitions to levels 8 and 9 ($3s3p^2\ ^2S_{1/2}$ and $^2P_{1/2}$). If these are excluded, the mean difference between our results at 10 Ryd and those of BK93 is only 6.1% and with the values given by M 94, 4.1%. In our calculation, these two levels interact strongly, mainly through the spin-orbit interaction and the strength of the interaction is, to a first approximation, inversely proportional to the energy separation between them. In the calculation of BK93, this separation is 34715 cm^{-1}, compared to the experimental value of 23832 cm^{-1} and our calculated value from Table 3 of 24267 cm^{-1}. We are therefore confident that the present work represents this interaction much more accurately than the results of BK93, and that consequently the distribution of collision strength between the $3s3p^2\ ^2S_{1/2}$ and $^2P_{1/2}$ levels is also more accurately represented. In DK91, target level energies are not given, but the collision strengths they obtain for the transitions between $3s^23p\ ^2P^o$ and $3s3p^2\ ^2S_{1/2}$ and $^2P_{1/2}$ are very similar to those obtained by BK93 at 10 Ryd and are therefore also significantly different to those presented here.

In Table 6 we compare collision strengths at 6 Ryd from an early distorted wave calculation by Mason (1975) with the results of DK91 and with the present work. At this energy, the calculations of Mason (1975) and DK91 can be compared directly, since the distorted wave method does not include resonance effects and the highest target threshold of DK91 lies lower at 4.198 Ryd. There are significant differences between the two calculations caused by the limited target expansion used in the earlier work (Mason 1975, 1994). In the present work, the highest target threshold lies at 7.681 Ryd, so there are resonance features present at 6 Ryd. The values given in Table 6 were derived from the calculated collision strengths by averaging over the energy range $5.5 - 6.5$ Ryd. These average values are significantly larger than the results of DK91, showing that resonances converging on the terms of the 3s3p3d electron configuration are important in this energy region.

In Fig. 1, we show the collision strength for the $3s^23p(^2P^o_{1/2}) - 3s3p^2(^2D_{5/2})$ transition, with the results in the resonance region averaged over 0.5 Ryd intervals. As described above, there is good agreement between the present work and that of DK91 in the non-resonant region above 8 Ryd, while at 6 Ryd, our results are significantly higher. The resonant enhancement seen in the collision strength in Fig. 1 between 4.3 and 7.7 Ryd is entirely due to the presence of the 3s3p3d electron configuration in the target. This enhancement is not accounted for in DK91 or BK93. It is evident from the figure that in this case, the contributions from the resonance region will be important in determining the thermally averaged collision strength as long as the mean thermal energy of the electrons is less than about 20 Ryd. This conclusion is confirmed by Fig. 2, which shows the thermally averaged collision strength for the $3s^23p(^2P^o_{1/2}) - 3s3p^2(^2D_{5/2})$ transition. We compare our current results with those obtained by DK91 and with values derived from the distorted wave collision strength data of BK93. Although the work of DK91 does include some resonance effects, it is clear

Table 5. Comparison of collision strengths above all thresholds

i	j		10 Ryd		30 Ryd	
		BK93†	M 94*	Present	BK93	Present
1	3	0.0170	0.016	0.0176	0.0140	0.0165
	4	0.0138	0.014	0.0127	0.0061	0.0062
	5	0.0105	0.010	0.0100	0.0045	0.0047
	6	0.716	0.717	0.735	0.859	0.931
	7	0.0257	0.025	0.0240	0.0141	0.0141
	8	0.986	0.991	1.316	1.208	1.701
	9	1.238	1.282	0.910	1.528	1.166
	10	0.924	0.954	0.906	1.135	1.162
	11	2.240	2.243	2.279	2.789	2.918
	12	0.0349	0.038	0.0392	0.0271	0.0293
2	3	0.0091	0.008	0.0086	0.0078	0.0080
	4	0.0202	0.020	0.0199	0.0123	0.0141
	5	0.0554	0.054	0.0579	0.0421	0.0512
	6	0.0843	0.082	0.0714	0.0732	0.0617
	7	1.146	1.133	1.131	1.357	1.395
	8	0.358	0.320	0.141	0.426	0.170
	9	1.368	1.414	1.550	1.677	1.954
	10	4.499	4.678	4.592	5.260	5.835
	11	0.626	0.630	0.619	0.762	0.764
	12	4.230	4.238	4.276	5.291	5.449

† Bhatia & Kastner (1993).
* Mason (1994).

Table 6. Comparison of collision strengths at 6 Ryd

i	j	Mason (1975)	DK91†	Present (average)
1	3	0.0178	0.0200	0.0249
	4	0.0136	0.0167	0.0265
	5	0.0103	0.0127	0.0272
	6	0.930	0.671	0.704
	7	0.0257	0.0237	0.0915
	8	1.103	0.9326	1.278
	9	1.667	1.208	0.888
	10	1.196	0.900	0.914
	11	2.800	2.117	2.485
	12	0.0411	0.0358	0.190
2	3	0.0085	0.0101	0.0190
	4	0.0211	0.0243	0.0425
	5	0.0616	0.0665	0.0944
	6	0.0986	0.0767	0.163
	7	1.483	1.062	1.157
	8	0.325	0.302	0.198
	9	1.690	1.334	1.527
	10	5.840	4.412	4.468
	11	0.783	0.594	0.827
	12	5.296	3.997	4.754

† Dufton & Kingston (1991).

that, for this transition, the most important resonance series are those converging on the 3s3p3d configuration which are absent in that calculation. Consequently, the results of DK91 are very similar to those of BK93 in which resonance effects are completely absent. We find similar resonance enhancements in all transitions between the $3s^23p$ and $3s3p^2$ configurations, when comparing to both the work of BK93 and that of DK91, with the largest enhancements being in those transitions which are intrinsically weak. The effective collision strength in the $3s^23p(^2P^o_{1/2}) - 3s3p^2(^4P_{5/2})$ transition, for example, is increased by a factor of 2.9 at $\log T = 6.2$. The strong allowed transitions are also enhanced, but by much smaller factors.

The increases in the collision strengths between the $3s^23p$ and $3s3p^2$ configurations will lead to corresponding increases in the populations of the levels of the $3s3p^2$ configuration. The populations of these levels will also be increased by excitation from the ground $3s^23p$ to the levels of the 3s3p3d configuration followed by radiative cascading to $3s3p^2$ and $3s^23d$. Again, the most strongly affected levels will be those whose excitation from the ground configuration is intrinsically weak. We return to this point is Sect. 6.

In Table 7, the final thermally averaged collision strengths for the strongest EUV transitions between the $3s^23p$ and the $3s3p^2$ and $3s^23d$ electron configurations are given as a function of electron temperature. The complete set of effective collision strengths among all of the forty levels listed in Table 3 are available in the electronic version of this paper.

5. Computing Fe XIV line intensities

In the following sections the new atomic data presented above will be used to compute line emissivities and these will be compared both with previous theoretical models and observations. In particular Y98 identified significant discrepancies between theory and observation when comparing the CHIANTI/v1.0 Fe XIV model (Sect. 4.14.2 of Dere et al. 1997) with data from the SERTS-89 instrument, Thomas & Neupert (1994) (hereafter TN94) and these issues will be directly addressed here.

5.1. Line emissivities

The line *emissivity*, ϵ_λ, is defined as

$$\epsilon_\lambda = \epsilon_{ij} = \Delta E\, N_j\, A_{ji} \quad (1)$$

for a transition between two levels of an ion with indices i and j that give rise to a line at wavelength λ. ΔE is the energy difference between the two levels, N_j is the number density of particles in the plasma that are in the emitting state of the ion, and A_{ji} is the radiative probability for the transition. When dealing only with lines emitted by a single ion, it is more convenient to define the *ion* emissivity as

$$\varepsilon_\lambda = \varepsilon_{ij} = \Delta E\, n_j\, A_{ji} \quad (2)$$

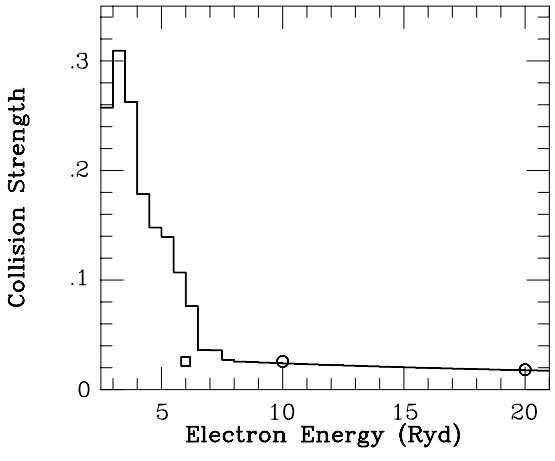

Fig. 1. Collision strength for the $3s^23p(^2P^o_{1/2}) - 3s3p^2(^2D_{5/2})$ transition. Solid line from present results averaged over 0.5 Ryd intervals. Open circles from Bhatia & Kastner (1993). Square from Dufton & Kingston (1991)

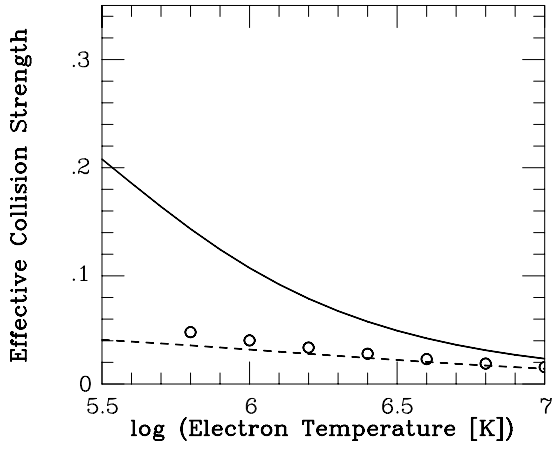

Fig. 2. Thermally averaged collision strength for the $3s^23p(^2P^o_{1/2}) - 3s3p^2(^2D_{5/2})$ transition. Solid line from present results, open circles from close-coupling calculation of Dufton & Kingston (1991), dashed line from distorted wave work of Bhatia & Kastner (1993)

where n_j is the fraction of the ions that are in the emitting state j.

For a plasma in steady state, in ionisation equilibrium and transparent to radiation, $\varepsilon_\lambda \propto I_\lambda$ where I_λ is the observed intensity of a line, and so one can directly compare ratios of ion emissivities with ratios of the line intensities.

To compute the n_j one needs to solve a set of linear equations which account for the atomic processes that populate and de-populate the levels of the ion. In the present work we will only consider electron excitation and de-excitation, and spontaneous radiative decay, to be consistent with the CHIANTI/v1.0 and B94 Fe XIV models that we shall be comparing with. Other processes that are significant in some circumstances are photorecombination, photoexcitation and stimulated emission by a background radiation field, and proton excitation–de-excitation, although their effects are generally small for Fe XIV emission from the solar atmosphere.

5.2. The Fe XIV models

Data from three Fe XIV models will be considered here and compared. The new model (to be referred to as SMY99) consists of the thermally averaged collision strengths from IP XIV for the ground transition, and those presented here for all other transitions. Radiative decay rates were calculated from the Basis 3 target referred to in Sect. 2. Level energies are the experimental values presented in Table 3.

This set of Fe XIV data will be included in a fitted form in a future release of the CHIANTI database. Following the format of the rest of the CHIANTI database, the electron collision data has been assessed and spline fitted with a method based on that of Burgess & Tully (1992; see also Sect. 3.4 of Dere et al. 1997). Thermally averaged collision strengths (Υ) have been computed over the temperature range $5.0 \leq \log T \leq 10.0$, and it was found that for many transitions the variation of Υ with T was too complex to be fitted with the 5-point spline that is the basis of the Burgess & Tully (1992) method. In these cases a restricted set of temperatures had to be considered. The range over which the fits are most accurate is $5.4 \leq \log T \leq 7.0$. Comparisons of Υ's derived from the spline fits with the original data generally give excellent agreement in this temperature range, with maximum differences of 5% in a few exceptional cases. The spline fit Υ's are those used by CHIANTI, and so the CHIANTI intensities should not be used outside the temperature range $5.4 \leq \log T \leq 7.0$.

Although collision strengths have been computed for all possible transitions between the forty levels of the present Fe XIV model, it is only necessary to consider the transitions that involve levels 1, 2 and 21 (see Table 3) as these are the only levels with significant population at typical coronal densities (Table 8). Thus only these transitions have been fitted.

The Fe XIV model contained in version 1.0 of the CHIANTI database was described in Dere et al. (1997) and will be referred to as CH97. This consisted of the 12 levels of the $3s^23p$, $3s\,3p^2$ and $3s^23d$ configurations, and thermally averaged collision strengths were taken from DK91 for the 3s−3p and 3p−3d transitions. For the ground transition, the IP XIV data were used. Radiative decay rates were from Froese Fischer & Liu (1986), and level energies were from the NIST database (Martin et al. 1995).

B94 presented an Fe XIV model that consisted of the DK91 electron collisional data for the 12 $3s^23p$, $3s\,3p^2$ and

Table 7. Thermally averaged collision strengths[†] for the strongest EUV transitions

i	j	log (T[K])							
		5.5	6.0	6.2	6.4	6.6	6.8	7.0	7.2
1	3	4.256(−2)	2.982(−2)	2.587(−2)	2.288(−2)	2.077(−2)	1.942(−2)	1.872(−2)	1.857(−2)
1	4	6.446(−2)	3.721(−2)	2.853(−2)	2.157(−2)	1.610(−2)	1.191(−2)	8.770(−3)	6.509(−3)
1	5	7.008(−2)	3.939(−2)	2.948(−2)	2.165(−2)	1.568(−2)	1.121(−2)	7.898(−3)	5.487(−3)
1	6	8.210(−1)	7.872(−1)	8.023(−1)	8.366(−1)	8.890(−1)	9.571(−1)	1.038(0)	1.129(0)
1	7	2.079(−1)	1.073(−1)	7.890(−2)	5.767(−2)	4.224(−2)	3.122(−2)	2.341(−2)	1.791(−2)
1	8	1.153(0)	1.293(0)	1.370(0)	1.469(0)	1.592(0)	1.738(0)	1.906(0)	2.090(0)
1	9	8.690(−1)	9.189(−1)	9.622(−1)	1.023(0)	1.102(0)	1.199(0)	1.312(0)	1.436(0)
1	10	8.846(−1)	9.271(−1)	9.670(−1)	1.025(0)	1.102(0)	1.198(0)	1.309(0)	1.432(0)
1	11	2.267(0)	2.369(0)	2.464(0)	2.607(0)	2.800(0)	3.042(0)	3.330(0)	3.654(0)
1	12	1.486(−1)	8.898(−2)	7.100(−2)	5.747(−2)	4.769(−2)	4.086(−2)	3.622(−2)	3.316(−2)
2	3	4.735(−2)	2.765(−2)	2.164(−2)	1.719(−2)	1.406(−2)	1.200(−2)	1.072(−2)	1.005(−2)
2	4	1.050(−1)	6.100(−2)	4.730(−2)	3.671(−2)	2.883(−2)	2.313(−2)	1.918(−2)	1.660(−2)
2	5	2.013(−1)	1.271(−1)	1.045(−1)	8.738(−2)	7.509(−2)	6.678(−2)	6.168(−2)	5.914(−2)
2	6	3.593(−1)	1.997(−1)	1.565(−1)	1.252(−1)	1.035(−1)	8.914(−2)	8.023(−2)	7.529(−2)
2	7	1.518(0)	1.320(0)	1.302(0)	1.321(0)	1.376(0)	1.459(0)	1.565(0)	1.690(0)
2	8	3.055(−1)	2.114(−1)	1.931(−1)	1.842(−1)	1.828(−1)	1.876(−1)	1.971(−1)	2.101(−1)
2	9	1.510(0)	1.576(0)	1.641(0)	1.734(0)	1.860(0)	2.015(0)	2.197(0)	2.399(0)
2	10	4.398(0)	4.637(0)	4.847(0)	5.144(0)	5.532(0)	6.008(0)	6.562(0)	7.179(0)
2	11	7.318(−1)	6.930(−1)	6.974(−1)	7.177(−1)	7.542(−1)	8.059(−1)	8.709(−1)	9.468(−1)
2	12	4.326(0)	4.474(0)	4.639(0)	4.892(0)	5.241(0)	5.684(0)	6.209(0)	6.806(0)

[†] In this and subsequent tables, 4.256(−2) denotes 4.256 10^{-2}.

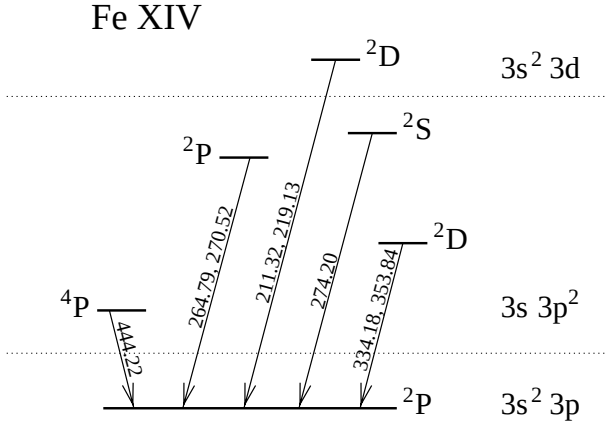

Fig. 3. A diagram illustrating the strongest EUV transitions. Wavelengths are given in Angströms

$3s^2 3d$ levels, and the BK93 distorted wave collision data for all transitions involving the 28 levels of the $3p^3$ and 3s 3p 3d configurations. The radiative data and level energies are from BK93. The same 5 configuration target that was used for the collisional model was used by BK93 for the radiative data, and so these are less accurate than both the Froese Fischer & Liu (1986) data and that used in the SMY99 model.

6. Comparing level populations

Level populations (the n_j of Sect. 5.1) were presented in B94 at densities $\log N_e = 8, 9, 10, 11, 12$ and temperatures $\log T = 6.0, 6.2, 6.4$, and we compare their results with the CH97 and SMY99 models in Table 8 at $\log N_e = 8, 10, 12$ and $\log T = 6.2$ for the most important Fe XIV levels. Using the original thermally averaged collision strengths rather than the spline fitted values changes these level populations by less than 1% over the temperature range of validity (see Sect. 5.2).

Although the populations of the two ground levels are very similar for the three different models, the other levels show differences of up to a factor 5. The differences with the CH97 model are due to the substantial cascading taking place from the higher levels, while the differences between the SMY99 and B94 models can be accounted for by the more accurate radiative data and the important resonance effects incorporated here (see Sect. 4).

7. Comparing theory and observations for the EUV lines

Fe XIV gives rise to a number of strong lines in the extreme ultraviolet (EUV; 150 − 900 Å) portion of the solar spectrum, the strongest of which are illustrated in Fig. 3 and listed in Table 9. These lines have been measured in a number of solar spectra, and we will use the published catalogues of Malinovsky & Heroux (1973, hereafter MH73) and TN94. The latter spectrum was obtained by the SERTS-89 instrument, and a detailed comparison of the CH97 Fe XIV model with these observations was presented in Sect. 13.6 of Y98, to which reference will be made in the following sections. In the following discussion we refer to wavelengths given in Table 9 rounded down

Table 8. A comparison of fractional level populations predicted from the three theoretical models (SMY99, B94, CH97; see Sect. 5.2). The values have been calculated for a temperature of log $T = 6.2$, and electron numbers densities of 10^8, 10^{10} and 10^{12} cm^{-3}

	log $N_e = 8$			log $N_e = 10$			log $N_e = 12$		
Index	SMY99	B94	CH97	SMY99	B94	CH97	SMY99	B94	CH97
1	9.85(−1)	9.85(−1)	9.86(−1)	5.44(−1)	5.49(−1)	5.53(−1)	3.52(−1)	3.56(−1)	3.53(−1)
2	1.51(−2)	1.45(−2)	1.40(−2)	4.54(−1)	4.46(−1)	4.47(−1)	6.33(−1)	6.31(−1)	6.47(−1)
3	2.78(−10)	2.21(−10)	1.18(−10)	2.06(−8)	1.48(−8)	8.35(−9)	1.74(−6)	1.20(−6)	6.76(−7)
4	2.05(−9)	1.74(−9)	7.39(−10)	1.81(−7)	1.49(−7)	6.60(−8)	1.76(−5)	1.42(−5)	6.23(−6)
5	5.98(−10)	4.29(−10)	1.28(−10)	7.42(−8)	5.98(−8)	2.21(−8)	7.88(−6)	6.43(−6)	2.64(−6)
6	1.02(−10)	7.82(−10)	6.63(−11)	6.27(−9)	4.85(−9)	3.99(−9)	4.55(−7)	3.53(−7)	2.76(−7)
7	2.58(−11)	1.73(−11)	5.34(−12)	6.75(−9)	4.84(−9)	3.36(−9)	8.40(−7)	6.17(−7)	4.67(−7)
8	1.83(−11)	9.74(−12)	9.42(−12)	1.08(−9)	6.96(−10)	6.71(−10)	7.57(−8)	5.71(−8)	5.45(−8)
9	6.94(−12)	7.09(−12)	9.59(−12)	6.56(−10)	5.27(−10)	7.16(−10)	6.32(−8)	4.45(−8)	6.03(−8)
10	6.09(−12)	4.23(−12)	5.30(−12)	1.00(−9)	6.88(−10)	8.72(−10)	1.16(−7)	7.99(−8)	1.03(−7)
11	1.26(−11)	9.14(−12)	1.10(−11)	7.79(−10)	5.65(−10)	6.85(−10)	5.68(−8)	4.10(−8)	4.91(−8)
12	7.11(−13)	3.70(−13)	3.66(−13)	6.43(−10)	4.30(−10)	5.20(−10)	8.76(−8)	5.97(−8)	7.43(−8)
21	6.51(−6)	4.07(−6)	–	2.39(−3)	4.75(−3)	–	1.51(−2)	1.30(−2)	–

to the nearest Angstrom; for example the intensity ratio $I_{252.20\ \text{Å}}/I_{264.79\ \text{Å}}$ is denoted as 252/264.

In comparing theory with observation, it is essential to consider the accuracy of the observed line intensities. The TN94 catalogue explicitly gives error bars for each observed line and these are used here. MH73 do not do this, but a discussion of the accuracy of the line intensities is given on p. 1019 of their work. Although some intensities may be accurate to only ±50%, the stronger lines are accurate to ≈ ±20%. Relative intensities of strong lines are expected to be rather more accurate than this. Here we will only use the measured intensities and not quote error bars, so the values just quoted should be borne in mind.

There are several line ratios that are suitable for determining the electron density and these will be discussed in Sect. 7.2. As a check on the accuracy of the atomic data, though, line ratios that are *insensitive* to the density will first be considered.

7.1. Density insensitive ratios

The importance of line ratios that are insensitive to the physical conditions in the solar atmosphere was stressed in Y98 with regard to the accuracy of both the atomic data and instrument calibration. In this work, such ratios were divided into branching ratios and density insensitive ratios. The branching ratios are those for which the two emission lines have a common emitting level in the ion, and so the ratio of their emissivities depends solely on the radiative data and the energy levels of the ion. A comparison amongst the different Fe XIV models is given in Table 10, and the ratios derived from the TN94 and MH73 spectra are also given. Similar values to those from the CH97 model are found here, indicating good agreement between the two sets of radiative data. The discrepancy identified by Y98 between theory and observations for the 257/270 is still not fully resolved. MH73 flag the 252 line as being blended, but do not identify the other component. It is likely, however, that the Fe XIV line lies in the wing of the stronger Fe XIII 251.95 Å line.

Density insensitive ratios arise through similarities in the way two lines are excited, e.g., if two lines are principally excited from the ground level at all densities, then their ratio will be insensitive to density. Four such ratios were identified in Y98, and are listed in Table 11. Theoretical values are listed for each of the three Fe XIV models considered here. These values have been compiled using a different method to that used by Y98 on account of the way the B94 data were presented. The value for the ratio is the value at log $N_e = 10.0$ and log $T = 6.2$, while the upper and lower limits represent the maximum deviations from this value over densities of $8.0 \leq \log N_e \leq 12.0$ and temperatures of $6.0 \leq \log T \leq 6.4$. Note that none of the ratios are strictly insensitive to density or temperature, but the variations are less than or comparable to the errors in the observations.

Based on the CH97 model, Y98 listed the 270/211 ratio as insensitive as it shows relatively small variation with density (Fig. 4). In the SMY99 model, however, the ratio shows significantly greater variability. The reason for this lies in the way the 270 line is excited. The upper level for the 270 transition is 9 (Table 9), and the ratio $\Upsilon_{2,9}/\Upsilon_{1,9}$ at log $T = 6.2$ is 1.71 from Table 7. The B94 and CH97 models contain upsilons from DK91 which give a ratio of $\Upsilon_{2,9}/\Upsilon_{1,9} = 0.82$ at log $T = 6.2$. Thus the way the 270

Table 9. Wavelengths and level identifications for the $3s^23p - 3s3p^2$ and $3s^23p - 3s^23d$ EUV permitted transitions

Transition				
Configurations	Terms	J-values	Indices	λ (Å)
$3s^23p - 3s\,3p^2$	$^2P - {}^4P$	$1/2 - 1/2$	1 – 3	444.22
		$3/2 - 1/2$	2 – 3	484.82
		$1/2 - 3/2$	1 – 4	429.57
		$3/2 - 3/2$	2 – 4	467.43
		$3/2 - 5/2$	2 – 5	447.36
	$^2P - {}^2D$	$1/2 - 3/2$	1 – 6	334.18
		$3/2 - 3/2$	2 – 6	356.65
		$3/2 - 5/2$	2 – 7	353.84
	$^2P - {}^2S$	$1/2 - 1/2$	1 – 8	274.20
		$3/2 - 1/2$	2 – 8	289.15
	$^2P - {}^2P$	$1/2 - 1/2$	1 – 9	257.39
		$3/2 - 1/2$	2 – 9	270.52
		$1/2 - 3/2$	1 – 10	252.20
		$3/2 - 3/2$	2 – 10	264.79
$3s^23p - 3s^23d$	$^2P - {}^2D$	$1/2 - 3/2$	1 – 11	211.32
		$3/2 - 3/2$	2 – 11	220.08
		$3/2 - 5/2$	2 – 12	219.13

Table 10. Emissivity ratios for lines with common upper levels

	Theory†			Observations	
Ratio	CH97	B94	SMY99	MH73[a]	SERTS-89[b]
220/211	0.21	0.22	0.22	0.28	0.25 ± 0.07
252/264	0.24	0.25	0.24	0.26	0.18 ± 0.06
257/270	0.75	1.12	0.66	n/a	0.38 ± 0.09
289/274	0.089	0.28	0.061	0.060	0.072 ± 0.024
356/334	0.036	0.048	0.029	n/a	0.028 ± 0.010

† Theoretical models CH97, B94, SMY99; see Sect. 5.2.
[a] Malinovsky & Heroux (1973).
[b] From Thomas & Neupert (1994).

line is excited is very different in the two cases, and leads to the 270/211 being density sensitive in the present case.

An interesting consequence of the change in behaviour of the 270 line is that the 274/270 ratio also now shows density sensitivity (Fig. 4). Y98 noted that the CH97 model gave the 274/270 ratio as insensitive, but that considerable variation was seen in observations, with values of between 1.3 and 2.3 quoted. As can be seen from Fig. 4, the ratio is now predicted to vary between 2.0 and 1.0, in excellent agreement with observations.

As another consequence of the change in behaviour of the 270 line, it is now found to be insensitive when taken relative to a sum of the 264 and 274 lines, and this ratio is now given in Table 11, where excellent agreement with the MH73 and SERTS-89 observations is found.

The 274/211 ratio was highlighted in Y98 as, although the lines are very strong in spectra from solar active regions, the observed ratio was almost *a factor 3* discrepant with theory. This problem is not fully resolved here, but the new theoretical ratio is ≈ 50% higher than the previous values, and is similar to the MH73 observed value. The Fe XIV 211 line was observed in second order by the SERTS instrument, and the question of whether the 1st–2nd order calibration may be in error has been raised in Brickhouse et al. (1995; Sect. 3.2.1) and Y98; Sect. 15.1. Brickhouse et al. suggest that the 2nd order lines may be too weak by around 50%, and we note this would lower the SERTS ratio to 0.67 in better agreement with the SMY99 model.

The 334/274 ratio found here is similar to that from the CH97 model, and agrees with the SERTS observations. The B94 ratio is, however, too high compared to observations. The 444/334 ratio is found to be higher than in the other models, in apparent disagreement with the SERTS-89 observations. However, in Sect. 15.1 of Y98 it was suggested that the SERTS-89 calibration should be revised for lines above 400 Å, on the basis of several density insensitive line ratios not agreeing with observed values. The Fe XIV 444/334 ratio (from the CH97 model) was one of only two that actually agreed with the original TN94 calibration. If we accept the revised calibration of Y98, then the SERTS-89 444/334 ratio becomes 0.036 ± 0.010 – in better agreement with the new Fe XIV model.

7.2. Density diagnostics

Four useful density diagnostics were identified by Y98 and we provide comparisons of the three different models considered here in Fig. 5, while densities derived from the Malinovsky & Heroux and SERTS-89 observations are presented in Table 12.

The agreement between the four ratios is excellent, and of particular interest is the 264/274 ratio, which Y98 noted yielded a very low density of $\log N_e \leq 8.4$ when the CH97 model was used. The new model now gives a density in agreement with other Fe XIV ratios (Table 12).

7.3. CDS observations

The Coronal Diagnostic Spectrometer (CDS) is one of the twelve instruments on board the Solar and Heliospheric Observatory (SOHO) and is described in Harrison et al. (1997). CDS observes at EUV wavelengths between 150 and 800 Å. There are two separate spectrometers, the grazing incidence (GIS) and the normal incidence (NIS). Calibration for the GIS is complicated and still somewhat uncertain, and we will consider only NIS spectra.

The 353/334 density diagnostic lines are observed by NIS and, indeed, they form one of the key density diagnostics for observers. A check on the quality of the

Table 11. Comparisons of density insensitive ratios for different models with observations

Lines	Theoretical ratios†			Observed ratios	
	CH97	B94	SMY99	MH73[a]	SERTS-89[b]
270/211	$0.48^{+0.13}_{-0.12}$	$0.42^{+0.10}_{-0.10}$		0.28	0.48 ± 0.09
274/211	$0.36^{+0.07}_{-0.08}$	$0.33^{+0.06}_{-0.07}$	$0.53^{+0.05}_{-0.03}$	0.60	1.01 ± 0.18
270/(264+274)			$0.26^{+0.02}_{-0.01}$	0.26	0.24 ± 0.04
334/274	$0.68^{+0.28}_{-0.13}$	$0.97^{+0.30}_{-0.14}$	$0.64^{+0.06}_{-0.04}$	n/a	0.62 ± 0.10
444/334	$0.015^{+0.006}_{-0.004}$	$0.017^{+0.004}_{-0.004}$	$0.028^{+0.011}_{-0.009}$	n/a	0.018 ± 0.005

† Theoretical models; CH97, B94, SMY99, see Sect. 5.2.
[a] Malinovsky & Heroux (1973).
[b] From Thomas & Neupert (1994).

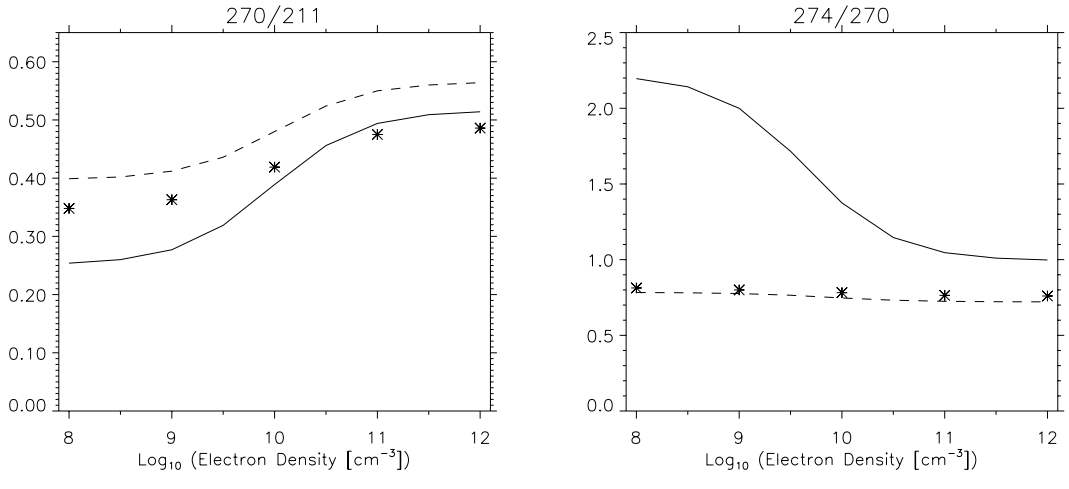

Fig. 4. Variation of the 270/211 and 274/270 ratios predicted from models; the solid line is present work; the dashed line is from CHIANTI/v1.0; the asterisks are from Bhatia et al. (1994)

atomic data is possible by looking at regions of low density (log $N_e \leq 9$) where the 353/334 ratio is close to the low density limit.

The ideal place to find low densities is above the limb in closed field regions. Here the plasma is close to being isothermal with temperatures of $6.1 \leq \log T \leq 6.3$, and so the Fe XIV lines are very prominent – see Fig. 6. Several data-sets containing the Fe XIV lines from such regions were selected and 353/334 ratios derived. The points in Fig. 7 show these values. Note that the NIS calibration was revised on 23-Dec.-98, and the values were derived with this new calibration.

Also plotted in this figure are horizontal lines representing the low density limits predicted by the three Fe XIV models. The SMY99 and B94 models predict the same value, while the CH97 model gives a value a factor of 4 lower. Note that for the CH97 and SMY99 models, the low density limit was calculated at log $T = 6.2$ and log $N_e = 1$, whereas the B94 value is the ratio value at log $N_e = 8$, the lowest density considered by B94. The actual low density limit is likely to be marginally less.

Table 12. Densities deduced from the SERTS-89 observed intensities using the present SMY99 model. Densities are in cm^{-3} and log $T = 6.3$

Ratio	SERTS-89[a]		MH73[b]	
	Ratio	log N_e	Ratio	log N_e
219/211	0.404 ± 0.082	$9.48^{+0.11}_{-0.14}$	0.186	9.01
264/274	1.010 ± 0.168	$9.36^{+0.20}_{-0.27}$	0.826	9.05
353/334	0.453 ± 0.073	$9.50^{+0.13}_{-0.16}$	*n/a*	–
447/444	2.882 ± 0.743	$9.60^{+0.53}_{-1.03}$	*n/a*	–

[a] From Thomas & Neupert (1994).
[b] Malinvosky & Heroux (1973).

The observations clearly show that the CH97 model disagrees with observations, being over a factor of 4 too low. Both the SMY99 and B94 models are in good agreement with the observed values.

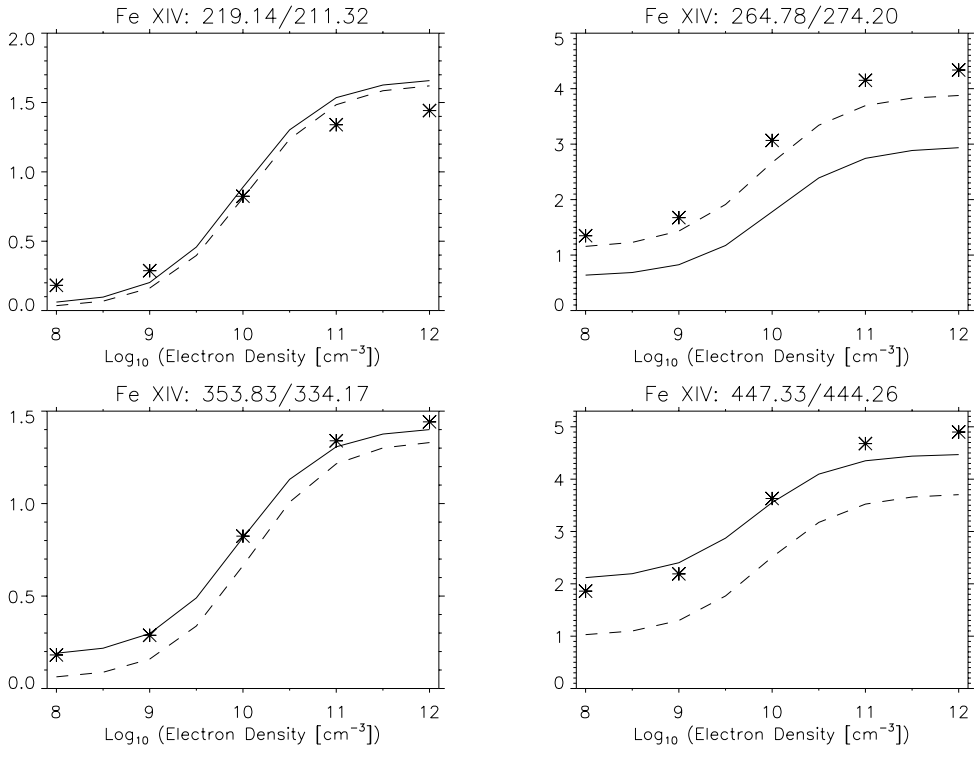

Fig. 5. Comparisons of the Bhatia et al. (1994) (asterisks), CHIANTI/v1.0 (dashed line) and present (complete line) calculations for four density diagnostic line ratios

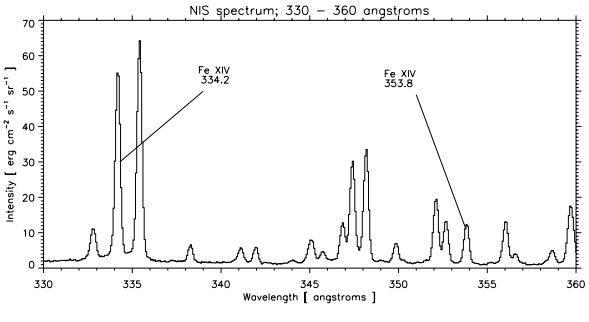

Fig. 6. NIS spectrum in the range 330 to 360 Å taken above an active region on the solar limb. The Fe XIV 334.2 and 353.8 Å lines are clearly seen

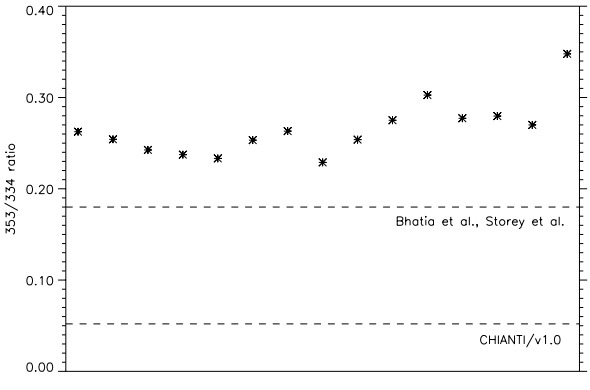

Fig. 7. A comparison of the low density limits of the Fe XIV 353/334 density diagnostic predicted by the three models considered here with observed values (stars in the figure) of the ratio in low density regions

8. Summary

The atomic calculations presented here are a significant advance over previous work. In particular, we have shown that resonances converging on the 3s3p3d electron configuration increase the thermally averaged collision strengths for several key diagnostic transitions.

Many of the discrepancies between observed and theoretical intensity ratios noted by Y98 for Fe XIV now seem to have been resolved. In particular we find the following results.

– The theoretical 274/211 ratio is now in good agreement with the MH73 spectrum. There is still a discrepancy with the TN94 spectrum, but this may be due to an inaccurate first/second order SERTS-89 calibration;
– The 264/274 ratio now gives densities in both the MH73 and TN94 spectra that are consistent with other Fe XIV ratios;
– The 270/274 ratio is found to be density sensitive, in contrast with previous models, and the range of

variation is in good agreement with a variety of observations;
- The low density limit of the 353/334 ratio is in good agreement with theory;
- The 444/334 ratio is now consistent with ratios from other ions which suggested that the SERTS-89 calibration is in error above around 400 Å. Previously this ratio was one of the few that suggested the calibration was not in error.

We recommend that our new atomic data be adopted for future analyses of solar and other astronomical spectra.

Acknowledgements. We acknowledge financial suport for the IRON Project from PPARC. SOHO is an NASA/ESA project. We thank the SOHO-CDS and SERTS teams for their assistance, in particular R.A. Harrison, C.D. Pike and R.J. Thomas.

References

Arnaud M., Raymond J.C., 1992, ApJ 398, 39
Berrington K.A., Burke P.G., Chang J.J., et al., 1974, Comput. Phys. Commun. 8, 149
Berrington K.A., Burke P.G., Le Dourneuf M., et al., 1978, Comput. Phys. Commun. 14, 367
Berrington K.A., Burke P.G., Butler K., et al., 1987, J. Phys. B 20, 6379
Bhatia A.K., Kastner S.O., 1993, J. Quant. Spectrosc. Radiat. Transf. 49, 609
Bhatia A.K., Kastner S.O., Keenan F.P., Conlon E.S., Widing K.G., 1994, ApJ 427, 497
Binello A.M., Mason H.E., Storey P.J., 1998, A&AS 131, 153
Brickhouse N.S., Raymond J.C., Smith B.W., 1995, ApJS 97, 551
Burgess A., Tully J.A., 1992, A&A 254, 436
Churilov S.S., Levashov V.E., 1993, Phys. Scr. 48, 425
Dere K.P., Landi E., Mason H.E., Monsignori-Fossi B.F., Young P.R., 1997, A&AS 125, 149
Dufton P.L., Kingston A.E., 1991, Phys. Scr. 43, 386
Eissner W.E., Jones M., Nussbaumer H., 1974, Comput. Phys. Commun. 8, 270
Froese Fischer C., Liu B, 1986, ADNDT 34, 261
Harrison R.A., Fludra A., Pike C.D., et al., 1997, Sol. Phys. 170, 123
Hummer D.G., Berrington K.A., Eissner W.E., et al., 1993, A&A 279, 298
Malinovsky M., Heroux L., 1973, ApJ 181, 1009
Martin W.C., Sugar J., Musgrove A., et al., 1995, NIST Database for Atomic Spectroscopy, Version 1.0, NIST Standard Reference Database 61
Mason H.E., 1975, MNRAS 170, 651
Mason H.E., 1994, ADNDT 57, 305
Mason H.E., Young P.R., Pike C.D., et al., 1997, Sol. Phys. 170, 143
Nussbaumer H., Storey P.J., 1978, A&A 64, 139
Redfors A., Litzén U., 1989, J. Opt. Soc. Am. B 6, No. 8, 1447
Saraph H.E., 1972, Comput. Phys. Commun. 3, 256
Saraph H.E., 1978, Comput. Phys. Commun. 15, 247
Storey P.J., Mason H.E., Saraph H.E., 1996, A&A 309, 672 (IP XIV)
Thomas R.J., Neupert W.M., 1994, ApJS 91, 461
Young P.R., Landi E., Thomas R.J., 1998, A&A 329, 291
Zeippen C.J., Seaton M.J., Morton D.C., 1977, MNRAS 181, 527